Cell membrane fluidity in the intact kidney proximal tubule measured by orientation-independent fluorescence anisotropy imaging

Kiyohide Fushimi, James A. Dix, and A. S. Verkman
Departments of Medicine and Physiology, Cardiovascular Research Institute, University of California, San Francisco, California 94143-0532

ABSTRACT Membrane fluidity was measured in the isolated perfused proximal tubule from rabbit kidney. The apical and basolateral plasma membranes of tubule cells were stained separately with the fluidity-sensitive fluorophore trimethylammonium-diphenylhexatriene (TMA-DPH) by luminal or bath perfusion. Fluorescence anisotropy (r) of TMA-DPH was mapped with spatial resolution using an epifluorescence microscope (excitation 380 nm, emission >410 nm) equipped with rotatable polarizers and a quantitative imaging system. To measure r without the confounding effects of fluorophore orientation, images were recorded with emission polarizer parallel and perpendicular to a continuum of orientations of the excitation polarizer. The theoretical basis of this approach was developed and its limitations were evaluated by mathematical modeling. The tubule inner surface (brush border) was brightly stained when the lumen was perfused with 1 μM TMA-DPH for 5 min; apical membrane r was 0.281 ± 0.006 (23° C). Staining of the tubule basolateral membrane by addition of TMA-DPH to the bath gave a significantly lower r of 0.242 ± 0.010 ($P < 0.005$); there was no staining of the bursh border membrane. To interpret anisotropy images quantitatively, effects of tubule geometry, TMA-DPH lifetime, fluorescence anisotropy decay, and objective depolarization were evalutated. Steady-state and time-resolved r and lifetimes in the intact tubule, measured by a nanosecond pulsed microscopy method, were compared with results in isolated apical and basolateral membrane vesicles from rabbit proximal tubule measured by cuvette fluorometry; r was 0.281 (apical membrane) and 0.276 (basolateral membrane) (23°C). These results establish a methodology to quantitate membrane fluidity in the intact proximal tubule, and demonstrate a significantly higher fluidity in the basolateral membrane than in the apical membrane.

INTRODUCTION

The polarized structure of renal epithelial cells is important for regulatory and transcellular transport functions. The lipid and protein composition of the opposing apical and basolateral plasma membranes differ greatly and are maintained by specific intracellular targeting and metabolic pathways. The renal proximal tubule consists of a single layer of homogeneous cells, arranged to form a cylinder of outside diameter ~40 μm. Cells are joined at their apical membranes by tight junctions. Numerous studies of membrane fluidity in purified apical and basolateral membrane vesicles from proximal tubule show differences in membrane fluidity and composition. The basolateral membrane has been suggested to have greater "fluidity" than the brush border membrane (Le Grimellec et al., 1983; Hise et al., 1984; Verkman and Ives, 1986; Molitoris and Hoilien, 1987); lifetime heterogeneity studies of parinaric acids showed a different structure of gel and fluid lipid domains (Illsley et al., 1988). Membrane fluidity of apical vesicles has been shown to be modulated by dietary phosphate, lipid content, animal age, and other factors (Chesney et al., 1986; Brasitus et al., 1984, 1986; Medow and Segal., 1987).

The purpose of this study was to measure the fluidity characteristics of the intact, viable proximal tubule. Unlike fluidity measurements in vesicles, studies in intact cells are not subject to isolation artifacts or membrane contamination, and can be used to measure continuously membrane fluidity in response to modification of the tubule physical or biochemical environment. Membrane fluidity was studied in isolated perfused proximal tubules from rabbit kidney using spatially resolved images of the fluorescence anisotropy of a fluidity-sensitive lipophilic fluorophore. The fluorophore trimethylammonium-diphenylhexatriene (TMA-DPH) was used in these studies because it stained the cell plasma membranes without significant internalization or passage across tight junctions (Prendergast et al., 1981; Le Grimellec et al., 1988). Because the complex geometry of the tubule plasma membrane resulted in dramatic effects of fluorophore orientation on apparent anisotropy values, an orientation-independent approach to measure anisotropy by quantitative imaging was developed, mathematically modeled, and experimentally validated. Results obtained in the

Address correspondence to Dr. A. S. Verkman.

intact tubule were compared with measurements of TMA-DPH anisotropy in purified apical and basolateral vesicles isolated from rabbit proximal tubule. In addition, nanosecond anisotropy decay and lifetime measurements in the intact tubule were obtained by a pulsed microscopy technique and compared with results in isolated membrane vesicles.

METHODS

Chemicals

1-(4-[trimethylamino]-phenyl)-6-phenyl-1,3,5-hexatriene (TMA-DPH), 1,6-diphenyl-1,3,5-hexatriene (DPH), and *N*-3-sulfopropyl-acridinium (SPA) were obtained from Molecular Probes (Eugene, OR). Phospholipids and other chemicals were obtained from Sigma Chemical Co. (St. Louis, MO). Low fluorescence immersion oil (type DF) was obtained from R. P. Cargile Laboratories, Inc. (Cedar Grove, NJ).

In vitro microperfusion system

Isolated segments of rabbit proximal straight tubule (PST) were dissected and perfused in vitro as described previously (Berry and Verkman, 1988; Kuwahara et al., 1988). Briefly, kidneys from New Zealand white rabbits (1.5–2.5 kg) were cut into 1–2-mm coronal slices. Segments of PST (1.5–2.5 mm long) were dissected with sharpened forceps in cooled buffer (2°C) and transferred to a bath of 80 μl volume constructed for rapid fluid exchange and stable flow (Strange and Spring, 1986). Dissected tubules were cannulated by aspirating the free ends into glass holding pipettes and advancing a concentric perfusion pipette ~100 μm into the lumen. Lumen perfusion was driven by a hydrostatic pressure of 20–25 cm H_2O. The bath solution was maintained at 23°C and exchanged continuously at 5 ml/min. Bath exchange time was under 1 s. The bath and perfusion solutions contained (in millimolar): 142 NaCl, 4 Na_2HPO_4, 0.8 NaH_2PO_4, 5 KCl, 1 $CaCl_2$, and 5 glucose (buffer A). Solution pH was adjusted to 7.4 by addition of HCl or NaOH.

Tubules were perfused with buffer A at 23°C for 15 min for metabolic stabilization. Tubule cells were labeled by perfusion with 0.5–2 μM TMA-DPH in buffer A from the lumen or bath solutions. Labeling was followed in real time by fluorescence microscopy. TMA-DPH was added to buffer A from a 1-mM stock solution in ethanol before each experiment.

Fluorescence imaging system

Fluorescence anisotropy imaging was performed on an apparatus described in the accompanying paper for application to randomly oriented fluorophores (Dix and Verkman, 1990). Fluorescently labeled tubules were viewed with an inverted epifluorescence microscope (Nikon Diaphot-TMD-EF, Nippon Kogaku, Tokyo, Japan) which was modified to measure fluorescence anisotropy quantitatively. Excitation light was polarized by a rotatable film polarizer. The excitation source consisted of a 100-W tungsten-halogen lamp in series with a KG-1 infrared blocking filter (Schott Glass, Duryea, PA) and 380 ± 5-nm six-cavity interference filter (Omega Optical, Inc., Brattleboro, VT). Light was reflected onto the perfusion bath by a 400-nm fused silica dichroic mirror (Omega Optical, Inc.). Three objectives were used in this study: 100× fluorotar (Nikon, NA 1.30, oil immersion, 0.17 mm working distance), 40× quartz (Leitz, NA 0.65, glycerol immersion, 0.35 mm working distance), and 16× quartz (Leitz, NA 0.25, 0.35 mm working distance). To place the tubule in the focal plane of the immersion objectives, the tubule was positioned near, but not touching, the glass coverslip (0.09 mm thick) which formed the bottom of the perfusion bath.

Emitted light was filtered by KV408 and GG420 cut-on filters (Schott Glass) and passed through a rotatable film polarizer to analyze fluorescence depolarization. The image was focused onto a variable gain, microchannel plate, image intensifier (Videoscope International, Washington, DC) and imaged with a solid-state CCD camera (Cohu Inc., San Diego, CA) operating at fixed gain. The output of the CCD camera was digitized with a frame grabber (model DT2861; Data Translation, Marlboro, MA) in a 80286 computer with 80287 math coprocessor (Rose Hill, Scotts Valley, CA) and an auxiliary processing board (model DT2858; Data Translation) to speed frame processing. Data acquisition and analysis software were written using the Fortran subroutine library supplied by Data Translation. Calculation of orientation-independent anisotropy images from 26 separate images (see below) required ~8 min of computational time.

Determination of anisotropy without orientation independence

For measurement of a spatially resolved anisotropy image, images were taken of the perfused tubule with the emission polarizers aligned parallel and perpendicular to the excitation polarizer. Background images of the tubule before TMA-DPH labeling were obtained for each polarizer orientation. To obtain an anisotropy image that did not depend upon orientation of the tubule with respect to the plane of excitation polarization, the parallel and perpendicular images were recorded for a series of orientations of the excitation polarizer. The specialized instrumental calibration procedures and calculations for this orientation-independent anisotropy imaging are presented in Results.

The imaging system was aligned and calibrated in every set of experiments. The excitation polarizer was set to a horizontal position (0° orientation) by maximizing detected light in the absence of an emission polarizer, making use of the polarization characteristics of the dichroic mirror. To align the emission polarizer, the dichroic mirror was replaced with a partially silvered mirror and the emission filters were removed; the emission polarizer was set to an angle of 90° and the mount was rotated until a minimum in reflected light intensity was obtained. For a single plane of excitation polarization, calculation of anisotropy from parallel and perpendicular sample and background images was performed as described in the accompanying paper (Dix and Verkman, 1990). The anisotropy image was displayed by pseudocolor. Anisotropy profiles across the width of the tubule were calculated from the anisotropy image by averaging anisotropy values over a 10–20-μm tubule length.

The accuracy of the anisotropy imaging system was tested in every set of experiments by imaging solutions of known anisotropy at the excitation and emission wavelengths of TMA-DPH. Calibration solutions consisted of 50 μM SPA in water (r = 0.011), 20 μM DPH in thin immersion oil (r = 0.105), and 20 μM DPH in viscous immersion oil (r = 0.253). The anisotropy of calibration solutions was determined by cuvette fluorometry (see below). Anisotropies obtained by the imaging system using the 40× or 16× quartz objectives agreed with the cuvette measurements to within 0.01 U.

Time-resolved microscopy measurements

Nanosecond lifetimes of TMA-DPH in the apical and basolateral membranes of the perfused proximal tubule were measured with the epifluorescence microscope interfaced to a pulsed lifetime instrument

(model LS-1; Photon Technology International (PTI), London, Ontario). The light source was a nitrogen-filled flashlamp operating at 5 kV and 300 mmHg pressure. The flash rate was 25 kHz. Excitation and emission filters were the same as that for steady-state measurements. Tubules were viewed with the 40× quartz objective. To minimize background signal, fluorescence was measured in a rectangular area over a 100-μm tubule length. Emitted light was detected by a gated photomultiplier which was turned on for 100 ps one time after each flash, at delay times of 0–30 ns after the beginning of the flash. The flashlamp profile was recorded before and after every fluorescence decay determination by measurement of reflected excitation light in the absence of an emission cut-on filter. Background decay data was determined by moving the tubule out of the rectangular measuring area. The background signal was <4% of the total signal; fitted lifetimes were not altered by subtraction of background. Fluorescence decay and lamp profile data were fitted to models containing ground-state heterogeneity by standard deconvolution procedures provided by PTI. Anisotropy decay was determined by measurement of fluorescence decay with emission polarizer oriented parallel and perpendicular to a continuum of orientations of the excitation polarizer (see Results).

Isolated vesicle experiments

Apical and basolateral membrane vesicles were isolated from rabbit renal proximal tubule by a gradient centrifugation method described previously (Illsley et al., 1988). Vesicles were suspended in buffer A at concentrations of 0.01–0.1 mg protein/ml. TMA-DPH (1:100 to 1:500 dye/lipid ratios) was added to the vesicle suspension while vigorously vortexing. The suspension was incubated in the dark under N_2 for 60 min at 23°C before measurements.

Steady-state anisotropy was measured in an SLM 48000 fluorometer (Urbana, IL) using Glan-Thompson polarizers in the T-format. Measurements were performed in a 10 × 2 mm quartz cuvette to minimize emission depolarization. Excitation was 380 ± 4 nm. Emission light was filtered by sequentially placed KV408 and GG420 cut-on filters. Sample temperature was controlled by a circulating water bath and monitored by a thermistor in the cuvette. Background signal obtained in the absence of fluorophore was <2% of signal measured with fluorophore.

Nanosecond lifetime and differential polarization measurements were performed by the phase-modulation method using the 325-nm line of a 7.5-mW He-Cd laser (Liconix, Sunnyvale, CA) as excitation source. Lifetimes were measured using >10 modulation frequencies (1–225 MHz) against a 1,4-bis(5-phenyl-2-oxazolyl) benzene (POPOP) reference solution (lifetime 1.35 ns). Anisotropy decay was measured by differential polarization in the T-format and analyzed as described recently (Calafut et al., 1989).

RESULTS

The goal of these studies was to measure and compare the membrane fluidity of the opposing apical and basolateral membranes of the intact kidney proximal tubule. From previous work, the fluidity-sensitive fluorophore TMA-DPH was used because it intercalates easily into the outer leaflet of the plasma membrane bilayer and undergoes little internalization or passage across tight junctions (Le Grimellec et al., 1988). The steady-state anisotropy of TMA-DPH and similar compounds provides a measure of local membrane "microviscosity" or fluidity.

The apical plasma membrane of tubule cells was labeled with 1 μM TMA-DPH by luminal perfusion. The basolateral plasma membrane was labeled by addition of 1 μM TMA-DPH to the bath. Fluorescence micrographs of the labeled tubules are shown in Fig. 1. Tubules were imaged using a 100× objective having a sharp focal plane. The tubule labeled from the lumen showed a band of bright fluorescence in the region of the apical membrane. The thickness of the band (~3 μm) was similar to the height of apical membrane microvilli (3 μm; Kaissling and Kriz, 1979). There was little fluorescence beyond the band, indicating that the basolateral membrane was not labeled. This appearance did not change after 30 min of perfusion with luminal TMA-DPH at 37°C. After labeling for 30 min, the fluorescence intensity of the band decreased by >85% upon perfusion of the lumen for 10 min with a 1-mM suspension of unilamellar phosphatidylcholine vesicles not containing TMA-DPH. Therefore labeling was reversible and little cellular internalization of TMA-DPH occurred. The tubule labeled from the bath showed no evidence of lumen staining even after 60 min. Therefore TMA-DPH had the proper location for examination of plasma membrane fluidity in the proximal tubule.

Fig. 2 shows calculated anisotropy images of the proximal tubule labeled from the lumen. Fluorescence was excited with vertically polarized light and measured with horizontal and vertical orientations of the emission polarizer. Images are shown of three different segments of the same perfused tubule having different orientations. The results were surprising for two reasons. First, the anisotropy values depended strongly on the orientation of the tubule axis. Second, at any point along the tubule, the anisotropy varied markedly across the tubule. Because

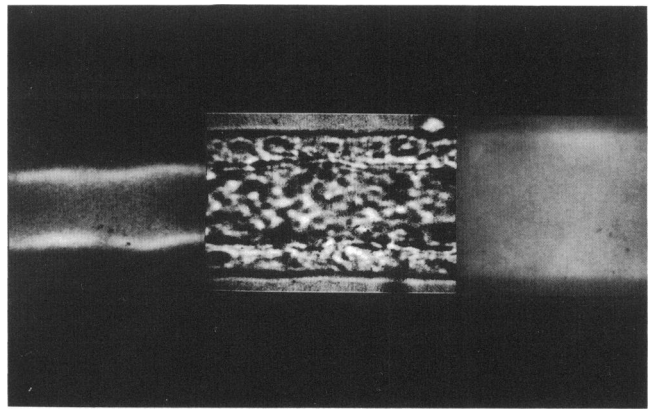

FIGURE 1 Brightfield (*middle*) and fluorescence (*left and right*) micrographs of perfused proximal tubules labeled for 10 min with 1 μM TMA-DPH at 23°C in the luminal solution (*left*) and bath solution (*right*). Tubules were viewed with the 100× oil immersion objective. Tubule diameter was 33 μm.

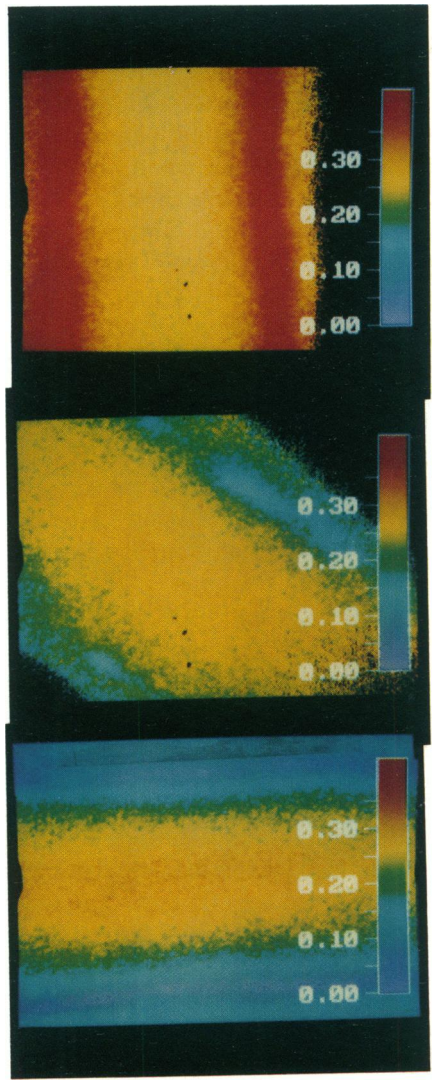

FIGURE 2 Anisotropy images of proximal tubule labeled with 1 μM TMA-DPH in the lumen solution. Tubules were viewed with the 100× oil immersion objective. Excitation polarization was in the x-z plane. Three anisotropy images are shown in different regions of the same perfused tubule where the angle between the polarization plane and tubule axis was 0° (*top*), 45° (*middle*), and 90° (*bottom*).

the apparent anisotropy depended on membrane fluidity and on tubule orientation and possibly other factors, it was necessary to evaluate the orientation dependence and to correct anisotropy values so that they would depend only on membrane fluidity.

Nonrandom fluorophore distributions could account qualitatively and quantitatively for the apparent anisotropy values. TMA-DPH is a linear fluorophore that intercalates in the lipid bilayer in a direction parallel to the phospholipids. The positively charged trimethylammonium moiety anchors the fluorophore to the polar surface of the outer bilayer leaflet to slow internalization by flip-flop. The excitation and emission dipoles of TMA-DPH are nearly colinear as shown by the limiting anisotropy (r_o) of 0.392 measured in the absence of depolarizing rotations. The apical membrane of the kidney proximal tubule consists of long cylindrical microvillus projections with a length of 3 μm and a diameter of 0.14 μm (Kaissling and Kris, 1979). The basolateral membrane of the kidney proximal tubule is also highly convoluted, but in a less ordered array. The basolateral membrane geometry has been compared with the trunk of a large tree; however, >50% of the total surface area is at the basal surface near the basement membrane.

Fig. 3 shows a schematic of the proximal tubule. The cylindrical microvilli are shown with TMA-DPH molecules oriented radially. To understand conceptually the mechanisms for the dependence of anisotropy on tubule orientation, assume that microvilli are uniform, aligned in the radial direction, and very long, and that the fluorophore is rigid with parallel excitation and emission dipoles. Consider the situation when the long axis of the tubule is parallel to the z-axis and excitation light is polarized in the y-z plane. At the edge of the tubule ($\gamma = 0$) the dipole axes of all fluorophores have a z-, but not an x-component. The apparent anisotropy under these conditions is 1. As γ increases from 0 to 90°, the fluorophore dipoles have an increasing component in the x-direction and a decreasing component in the z-direction. At 90°, anisotropy would approach 0.4 because the fluorophore dipoles are oriented randomly around the y-axis.

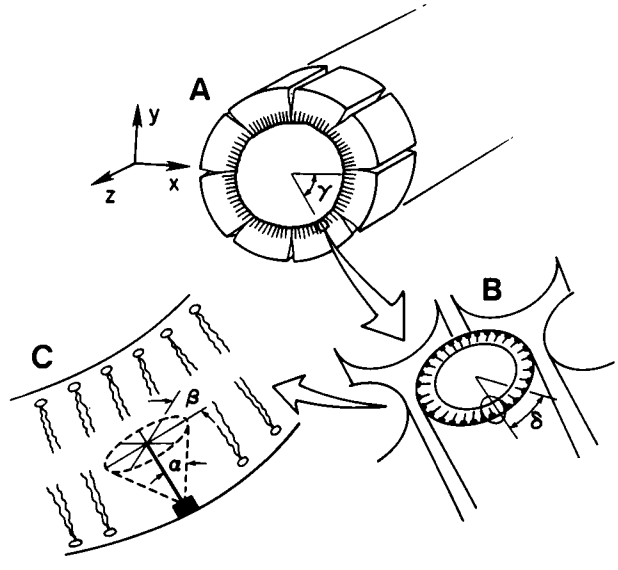

FIGURE 3 Schematic of proximal tubule labeled with TMA-DPH. (*A*) The tubule is a single layer of homogeneous cells with cylindrical microvillus projections of the apical (brush border) membrane. (*B*) Cross-section of a single microvillus showing radial orientation of TMA-DPH molecules incorporated into the outer leaflet of the lipid bilayer. (*C*) Expansion of the apical membrane showing phospholipids and a single TMA-DPH molecule rotating through an angle α.

Therefore, the apparent anisotropy decreases from the edge to the center of the tubule. The actual extremes in anisotropy are smaller than these values because of imperfect microvillus and fluorophore alignment, fluorophore depolarizing rotations, and contributions from out-of-focus fluorescence. When the axes of the tubule and excitation light are perpendicular, the situation is reversed. Anisotropy is lowest at $\gamma = 0°$ and highest at 90°. The dependence of measured anisotropy on the orientation of the excitation polarization is modeled quantitatively in Appendix 1. Tubule geometry, effects of depolarizing fluorophore rotations, and out-of-focus effects were included in the calculation. There was reasonable agreement between the theoretical calculation and the experimental data (see Appendix 1).

Orientation-independent fluorescence anisotropy imaging

Theory

It is clear that uncertainties in fluorophore and microvillus geometry and alignment make the correction of anisotropy images for orientation effects difficult. It was necessary to develop an approach to approximate the "true fluorophore anisotropy," without tubule orientation effects, so that the anisotropy of each fluorophore would be that measured in the hypothetical situation that the fluorophore was oriented randomly in three dimensions. An exact solution to this problem would require anisotropy measurements at all orientations of the sample in three dimensions (Burghardt, 1984; van Gurp et al., 1988). This was not a workable approach in practice. We have developed an approximate method to image the "true anisotropy" which becomes exact in the limit of parallel excitation and emission dipoles, and small angles of fluorophore depolarizing rotations. Fluorophore orientations in the x-z plane were averaged by "integrating" images obtained at all orientations of the excitation polarizer. The orientation-averaged anisotropy images, taken together with the cylindrical symmetry of kidney tubules, will enable quantitative comparisons to be made about differences in fluidity between the proximal tubule apical and basolateral membranes.

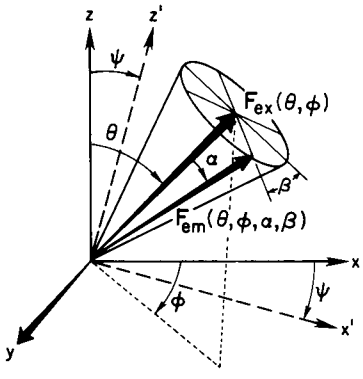

FIGURE 4 Optical arrangement for orientation-independent fluorescence anisotropy imaging. The excitation ($\mathbf{F}_{ex}$) and emission ($\mathbf{F}_{em}$) vectors of a single TMA-TPH fluorophore are shown. The coordinates θ and ϕ are referenced to the x, y, z axes. α is the angle between $\mathbf{F}_{ex}$ and $\mathbf{F}_{em}$. ψ is the angle between the z and z' axes in the x-z plane. See text for further explanation.

To eliminate the effect of fluorophore orientations in the x-z plane, the tubule was excited serially at all orientations of the excitation polarizer. Fig. 4 shows a fluorophore with excitation dipole $\mathbf{F}_{ex}(\theta, \phi)$. Light emitted at a later time has emission dipole $\mathbf{F}_{em}(\theta, \phi, \alpha, \beta)$. α is the angle between the excitation and emission dipoles[1] and β specifies the direction in which the depolarizing rotation occurs. The fluorophore is excited with polarized light in the y-z' plane, where ψ specifies the angle between the z- and z'-axes obtained by rotation around the y-axis.

The (x, y, z) components of vectors $\mathbf{F}_{ex}$, $\mathbf{F}_{em}$, $\mathbf{z}'$, and $\mathbf{x}'$ are:

$$\begin{aligned}
\mathbf{F}_{ex} &= (\sin\theta\sin\phi, \sin\theta\cos\phi, \cos\theta)\\
\mathbf{F}_{em} &= (\cos\alpha\sin\theta\sin\phi + \sin\alpha\cos\beta\cos\theta\sin\phi\\
&\quad + \sin\alpha\sin\beta\cos\phi, -\sin\alpha\sin\beta\sin\phi\\
&\quad + \sin\alpha\cos\beta\cos\theta\cos\phi\\
&\quad + \cos\alpha\sin\theta\cos\phi, -\sin\alpha\cos\beta\sin\theta\\
&\quad + \cos\alpha\cos\theta) \qquad (1)\\
\mathbf{z}' &= (\sin\psi, 0, \cos\psi)\\
\mathbf{x}' &= (\cos\psi, 0, -\sin\psi).
\end{aligned}$$

For excitation light in the y-z' plane, emitted fluorescence is measured at orientations of the emission polarizer parallel to the z' and x' axes. The dependence of anisotropy on the orientation of $\mathbf{F}_{ex}$ in the x-z plane is eliminated by integration over the angle ψ. The averaged parallel $\langle I_\parallel \rangle$ and perpendicular $\langle I_\perp \rangle$ components of emission fluorescence are:

$$\langle I_\parallel \rangle = \int_0^\pi d\psi \int_0^{2\pi} d\beta\, (\mathbf{F}_{ex} \cdot z')^2\, (\mathbf{F}_{em} \cdot z')^2 \qquad (2a)$$

$$\langle I_\perp \rangle = \int_0^\pi d\psi \int_0^{2\pi} d\beta\, (\mathbf{F}_{ex} \cdot z')^2\, (\mathbf{F}_{em} \cdot x')^2. \qquad (2b)$$

For an ensemble of excitation dipoles with orientation density function $D(\theta, \phi)$ (see Appendix 2), the integrands in Eqs. 2a and b are multiplied by $D(\theta, \phi)$ and integration over θ and ϕ is carried out. The calculated anisotropy, r =

[1]The angle α is taken to be a time-averaged angular displacement between the excitation and emission dipoles which depends upon fluorescence lifetime and anisotropy decay. This is a reasonable approximation because there is no established theory to relate the kinetics of rotational diffusion to measured anisotropy decay.

$(\langle I_\parallel \rangle - \langle I_\perp \rangle)/(\langle I_\parallel \rangle + 2\langle I_\perp \rangle)$, for a single dipole (where $D[\theta, \phi]$ is a delta function of θ and ϕ) is,

$$r = \frac{2(\cos^2\theta\cos^2\phi - \cos^2\phi + 1)^2(3\cos^2\alpha - 1)}{3(5\cos^2\theta\cos^2\phi - 5\cos^2\phi + 1)\cos^2\alpha - 5\cos^2\theta\cos^2\phi + 5\cos^2\phi + 7} \quad (3)$$

Because the y-component of $\mathbf{F}_{ex}$ (normalized to unity length) is $y = \sin\theta \cdot \cos\phi$, Eq. 3 can be simplified,

$$r = \frac{2(1 - y^2)(3\cos^2\alpha - 1)}{3(1 - 5y^2)\cos^2\alpha + 5y + 7}. \quad (4)$$

Fig. 5 shows the relationship between r/r_{ran} vs. y, where r_{ran} is the anisotropy of a hypothetically randomly orientated fluorophore equal to $(3\cos^2\alpha - 1)/5$. As expected, integration of Eqs. 2a and b for a random fluorophore distribution ($D(\theta, \phi) = \sin\theta\, d\theta\, d\phi$) gives r_{ran}. In the absence of depolarizing rotations ($\alpha = 0°$), r is 0.4. In general, r is different from r_{ran} for $\alpha > 0°$ because of the asymmetric effect of isotropic fluorophore rotations on the depolarization of excitation light. This effect is greatest for large α and when $\mathbf{F}_{ex}$ is oriented out of the x-z plane (large y).

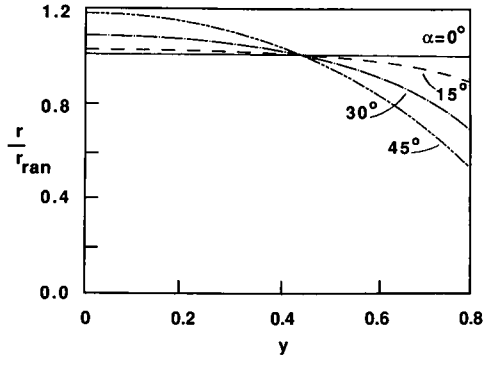

FIGURE 5 Dependence of measured anisotropy on the component of $\mathbf{F}_{ex}$ in the y-direction and on α. r_{ran} is the anisotropy in the hypothetical situation that the fluorophore were randomly oriented in space. Curves calculated from Eq. 4.

Measurement of orientation-independent anisotropy

Experimentally, the two methods to alter the angle between the tubule and excitation polarization axes are to rotate the tubule or to rotate the plane of excitation polarization. The former method is not practical because the complex and delicate perfusion apparatus cannot be rotated easily, and because of difficulties in rotating and aligning measured images. The second method was chosen.

The excitation polarizer was rotated to a set of discrete angles, 15° apart, between 0° and 180° (Fig. 6). At each

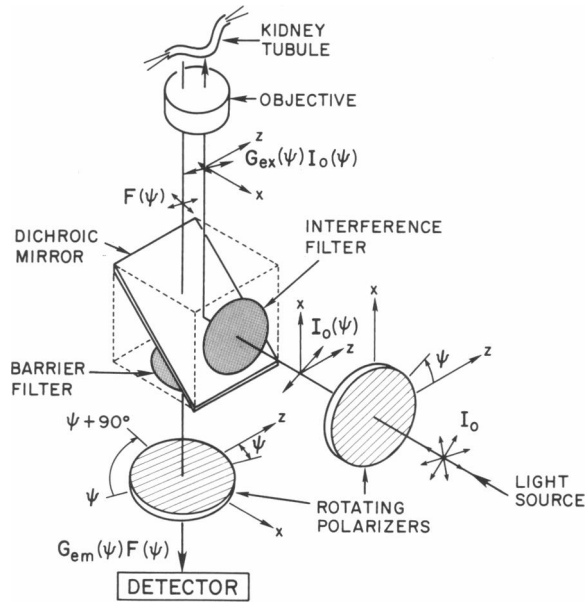

FIGURE 6 Optical path of the anisotropy imaging system containing rotatable excitation and emission polarizers. See text for explanation.

angle of the excitation polarizer, ψ, background and sample images were recorded at angles ψ and $\psi + 90°$ of the emission polarizer. The orientation-independent anisotropy $\langle r_{i,j} \rangle$ at each pixel was calculated from the equation:

$$\langle r_{i,j} \rangle = (1 - \langle I_{\perp i,j} \rangle / \langle I_{\parallel i,j} \rangle)/(1 + 2\langle I_{\perp i,j} \rangle / \langle I_{\parallel i,j} \rangle), \quad (5)$$

where $\langle I_{\parallel i,j} \rangle$ and $\langle I_{\perp i,j} \rangle$ are the ψ integrated parallel and perpendicular components of emitted fluorescence that have been corrected for background and instrumental polarization effects:

$$\langle I_{\parallel i,j} \rangle = \sum_{\psi=0}^{\pi} a(\psi) I_{\parallel i,j}(\psi); \quad \langle I_{\perp i,j} \rangle = \sum_{\psi=0}^{\pi} a(\psi) I_{\perp i,j}(\psi). \quad (6)$$

$a(\psi)$ are quadrature coefficients for numerical integration by the parabolic method. $I_{\parallel i,j}(\psi)$ and $I_{\perp i,j}(\psi)$ are determined from measured sample, $S_{i,j}(\psi)$, and background, $B_{i,j}(\psi)$, images by the relation:

$$\begin{pmatrix} S_{\parallel i,j} - B_{\parallel i,j} \\ S_{\perp i,j} - B_{\perp i,j} \end{pmatrix} = \begin{bmatrix} G_{em}(1,1) & G_{em}(1,2) \\ G_{em}(2,1) & G_{em}(2,2) \end{bmatrix} \cdot \begin{pmatrix} I_\parallel & I_\perp \\ I_\perp & I_\parallel \end{pmatrix} \begin{bmatrix} G_{ex}(1,1) & G_{ex}(1,2) \\ G_{ex}(2,1) & G_{ex}(2,2) \end{bmatrix} \begin{pmatrix} 1 \\ 0 \end{pmatrix}. \quad (7)$$

$\mathbf{G}_{ex}(\psi)$ and $\mathbf{G}_{em}(\psi)$ are rotation tensors that contain terms to correct measured fluorescence intensities for the polarization properties of the microscope components. As shown in Fig. 6, 100% polarized excitation light at an angle ψ, $\mathbf{I}_o = (1, 0)$, strikes the dichroic mirror. The reflection efficiencies of the dichroic mirror depend

weakly upon ψ. In addition, the dichroic itself causes slight depolarization of the excitation light (0.5–5% for ψ = 0–45°). These effects were minimized empirically by selection of a special fused silica 400-nm dichroic mirror. The light striking the tubule, $\mathbf{G}_{ex}(\psi)\ \mathbf{I}_o$, excites fluorescence. The matrix of $I_\parallel(\psi)$ and $I_\perp(\psi)$ values, $\mathbf{I}(\psi)$, describes the fluorophore-induced depolarization of the parallel and perpendicular components of $\mathbf{G}_{ex}(\psi)\ \mathbf{I}_o$, where $\mathbf{F}(\psi) = \mathbf{I}(\psi)\ \mathbf{G}_{ex}(\psi)\ \mathbf{I}_o$. The fluorescence measured at the detector at positions ψ and $\psi + 90°$ of the emission polarizer, $\mathbf{S}(\psi) - \mathbf{B}(\psi) = (S_{\parallel i,j} - B_{\parallel i,j}, S_{\perp i,j} - B_{\perp i,j})$, is the product of $\mathbf{G}_{em}(\psi)$ and $\mathbf{F}(\psi)$. From these definitions and the symmetry of $\mathbf{G}_{ex}$ and $\mathbf{I}(\psi)$, the desired parameters $I_{\parallel i,j}$ and $I_{\perp i,j}$ were determined by the relation:

$$\mathbf{I}(\psi)\mathbf{I}_o = \mathbf{G}_{ex}(\psi)^{-1}\mathbf{G}_{em}(\psi)^{-1}[\mathbf{S}(\psi) - \mathbf{B}(\psi)]. \quad (8)$$

The correction tensors $\mathbf{G}_{em}(\psi)$ and $\mathbf{G}_{ex}(\psi)$ were determined by a calibration procedure for ψ = 0–180° in 15° intervals. $\mathbf{G}_{em}(\psi)$ was evaluated in two steps. First, the transmission and detection of parallel polarized light was measured from the fluorescence of DPH in hexane in the absence of an excitation polarizer and at angles of 0–180° of the emission polarizer. Second, the depolarization of light by the emission optics was determined by illuminating the objective from above with 100% polarized light at the emission wavelength and measuring the parallel and perpendicular components of detected signal. The maximum emission depolarization was 5% when ψ = 45°. $\mathbf{G}_{ex}(\psi)$ was evaluated in two steps. First, the transmission of parallel polarized light was measured from the fluorescence of DPH in hexane at parallel orientations of the excitation and emission polarizers. Second, depolarization of the excitation optics was measured from the parallel and perpendicular components of fluorescence detected with the filter cube inverted so that polarized excitation light was reflected directly onto the detector. There was no depolarization of light at 380 nm by the optical components distal to the dichroic mirror. Table 1 shows that the composite correction tensor $\mathbf{G}_{ex}(\psi)^{-1}\ \mathbf{G}_{em}(\psi)^{-1}$ has small off-diagonal elements, particularly near ψ = 0° and 90°.

The application of the correction tensor for r determination was validated by measurement of r for SPA in water and DPH in a moderately and highly viscous oil at different values of ψ (Table 2). The results show that r can be determined accurately at all angles of the excitation polarizer by correction for the small instrumental polarization artifacts. As shown below, further validation of the correction procedure was provided by the ability to obtain orientation-independent anisotropy images of tubules.

TABLE 1 Components of the composite correction tensor $\mathbf{G}_{ex}(\psi)^{-1}\mathbf{G}_{em}(\psi)^{-1}$

ψ	$t_{(1,1)}$	$t_{(1,2)}$	$t_{(2,1)}$	$t_{(2,2)}$
0°	1.222	−0.011	−0.017	1.011
15	1.243	−0.032	−0.041	1.053
30	1.277	−0.098	−0.105	1.158
45	1.269	−0.150	−0.148	1.271
60	1.209	−0.132	−0.125	1.315
75	1.118	−0.054	−0.043	1.318
90	1.089	−0.019	−0.013	1.319
105	1.124	−0.059	−0.047	1.327
120	1.203	−0.130	−0.120	1.325
135	1.271	−0.148	−0.150	1.269
150	1.266	−0.102	−0.107	1.164
165	1.235	−0.029	−0.037	1.047

$t_{(i,j)}$ is the component at row i and column j of matrix $\mathbf{G}_{ex}(\psi)^{-1}\mathbf{G}_{em}(\psi)^{-1}$.

Orientation-independent anisotropy images of proximal tubule

Fig. 7 shows anisotropy images of tubules labeled with TMA-DPH at the apical and basolateral membranes. Tubules were viewed with the 40× quartz objective (glycerol immersion, NA 0.65) so that multiple tubule orientations could be examined simultaneously. The top images were obtained by brightfield light microscopy. The anisotropy images in the middle were obtained with fixed excitation polarization in the x-z plane. An image threshold was set to visualize pixels with intensities well above background. The tubule with apical labeling appears to be narrow because only microvilli at the tubule lumen were stained. There was a marked dependence of measured anisotropy on the tubule orientation. The variation in anisotropy along the length of the tubule was eliminated in the orientation-independent images at the bottom of the figure. It would not be possible to obtain this result if there were a systematic artifact in the protocol for determination of an orientation-independent anisotropy image.

To examine whether significant objective depolarization occurred because of the ability of high numerical

TABLE 2 Measured anisotropy values of DPH in viscous and thin immersion oil and SPA

ψ	Viscous immersion oil	Thin immersion oil	SPA
0°	0.250	0.103	0.007
15	0.246	0.100	0.002
30	0.243	0.103	−0.001
45	0.237	0.103	0.000
60	0.253	0.109	0.002
75	0.254	0.109	0.001
90	0.253	0.107	−0.001

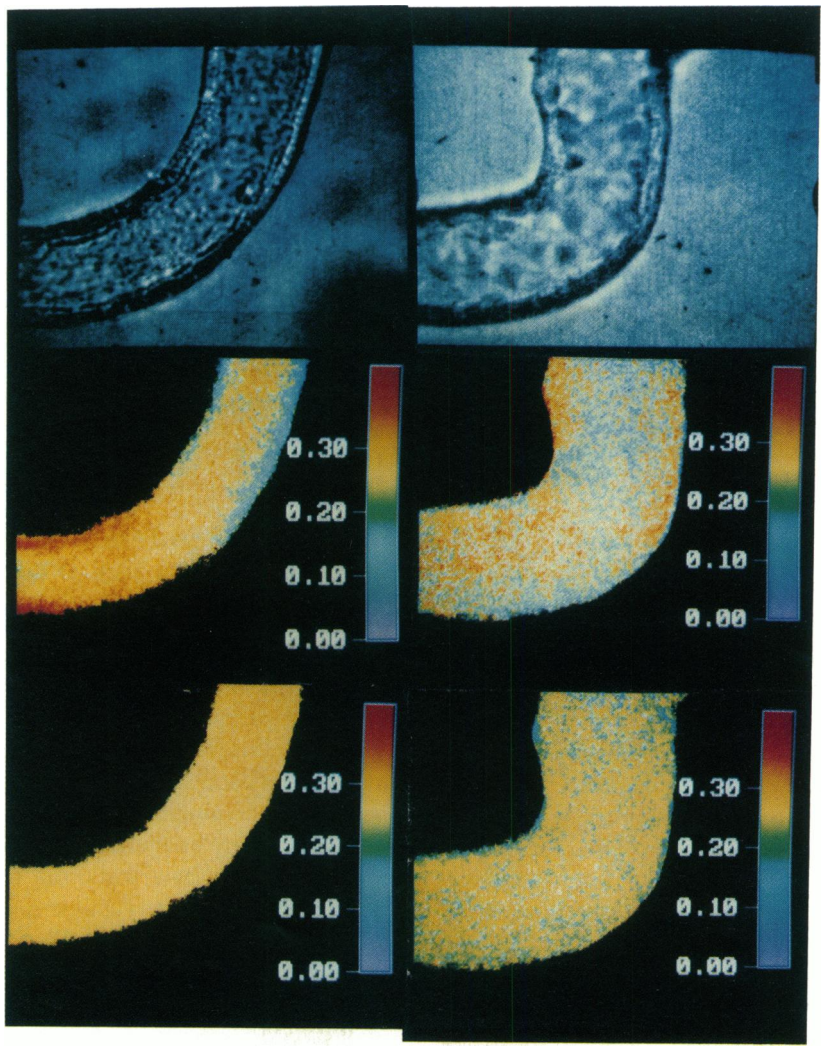

FIGURE 7 Orientation-independent anisotropy images of kidney proximal tubule. Tubules were labeled with 1 μM TMA-DPH from luminal (*left*) and bath (*right*) solutions and imaged using the 40× quartz objective. (Top) Brightfield images. (Middle) Anisotropy image obtained using excitation polarization in the horizontal plane. (Bottom) Orientation-independent anisotropy images. Tubule diameter was 36 μm.

aperture objectives to "see around" corners (Axelrod, 1979, 1989), the tubule on the left (apically stained) was imaged with the 100×, 40×, and 16× objectives. The calculated mean anisotropy over the tubule was decreased by 0.03 by use of the high NA objective (100×), but was not significantly different (<0.005) by use of the low NA objective (16×), indicating little effect of objective depolarization in images obtained with the 40× quartz objective.

In a single tubule, the typical standard deviation for the distribution of anisotropy values in separate pixels of the image at any fixed distance from the edge of the tubule was 0.01. There was no systematic variation in anisotropy along the length of the tubule. In three tubules stained with TMA-DPH in the apical membrane at 23°C, the average r was 0.281 ± 0.006 (SE). The r value was 0.242 ± 0.01 for staining of the basolateral membrane ($P < 0.005$). Importantly, there was <0.01 variation in r across the tubule, and as shown in Appendix 2, r_{ran} is between the maximum and minimum r across the tubule.

As evaluated in Fig. 5, out-of-plane fluorophore orientations influence the orientation-independent r values. To establish limits on the maximum and minimum values for r_{ran} in the apical and basolateral membranes, the cylindrical symmetry of the tubule was invoked (Appendix 2). In this calculation, a generalized orientation density function described by two parameters was developed. The presence of cylindrical symmetry requires mathematically that the orientation density functions at different points around the tubule are related by a rotational

matrix. The conclusions from the analysis in the Appendix are that apical membrane r must be between 0.276 and 0.315 with a corrected r (representing r_{ran}) of 0.281; basolateral membrane r must be between 0.237 and 0.282 with a corrected r of 0.244.

Control experiments were performed to show that anisotropy values were independent of the TMA-DPH concentration and incubation time. When luminal [TMA-DPH] was 0.5, 1, and 2 μM, anisotropy values were 0.29, 0.28, 0.29, respectively (SD range 0.008–0.012). At 1 μm TMA-DPH, anisotropies were 0.29 immediately after loading, and 0.28 after 30 min.

Fluidity measurements in isolated apical and basolateral membrane vesicles

Steady-state anisotropy, lifetime, and anisotropy decay measurements were performed on membrane vesicles labeled with TMA-DPH. The results are summarized in Table 3. Steady-state anisotropy was slightly, but significantly higher in apical than in basolateral vesicles. In three sets of vesicles, r for apical vesicles was 0.004–0.01 > r for basolateral vesicles. Control studies showed that r values were not influenced by the dye/lipid ratio or by emission scattering under the experimental conditions. This small increase in r in apical vesicles is similar to the 0.01 difference reported for TMA-DPH in apical and basolateral membrane vesicles from rat renal cortex (Molitoris and Hoilien, 1987). Differences in anisotropy between the apical and basolateral membranes were less marked in the vesicles than in the intact proximal tubule.

Lifetime measurements were performed to determine whether differences in steady-state anisotropy were due to differences in TMA-DPH lifetime. Lifetime analysis showed a small degree of ground-state heterogeneity without significant differences in values obtained for TMA-DPH in apical and basolateral membrane vesicles. Anisotropy decay was evaluated by the multifrequency phase-modulation method. It is predicted that TMA-DPH rotation should be isotropic because of its cylindrical symmetry. Differential polarization data were fitted well by an isotropic hindered rotational model. The effective rotational "cone angle" calculated according to Engel and Prendergast (1981) was 31°, showing that rotation of TMA-DPH is significantly hindered in the membrane.

Lifetime microscopy measurements in the intact tubule

The time-resolved decay of TMA-DPH fluorescence was measured over a 200-μm length of perfused tubule labeled from the luminal and bath solutions as described in Methods. The same optics were used for these studies except for replacement of the tungsten-halogen lamp by a nanosecond nitrogen flashlamp, and replacement of the image intensifier by a gated photomultiplier. The decay of TMA-DPH fluorescence in the labeled tubule is shown in Fig. 8 (*top*). Data were fitted well ($\chi^2 < 1.05$) to a model with a single exponential decay component. Fitted lifetimes given in Table 3 were slightly less than the longer lifetime component measured for TMA-DPH in membrane vesicles. The lifetime of TMA-DPH in the apical membrane did not differ significantly from that in the basolateral membrane. These results support the interpretation that differences in steady-state anisotropy are due to differences in membrane fluidity.

Orientation-independent anisotropy decay was performed by measurement of the nanosecond fluorescence decay at seven different orientations of the excitation polarizer, each with parallel and perpendicular orientations of the emission polarizer. Corrected, orientation-independent parallel and perpendicular fluorescence decay profiles were calculated from Eqs. 6 and 8, where

TABLE 3 Lifetime and steady-state anisotropy of TMA-DPH in vesicles and in tubules

System	Anisotropy	Lifetimes*			Rotational motion‡	
		τ_1	τ_2	f_1	τ_c	r_∞
		ns	*ns*		*ns*	
Apical, vesicles	0.281 ± 0.001	6.7 ± 0.2	1.6 ± 0.03	0.91 ± 0.04	0.4 ± 0.1	0.22 ± 0.01
Basolateral, vesicles	0.276 ± 0.001	6.7 ± 0.3	1.1 ± 0.02	0.96 ± 0.02	0.5 ± 0.1	0.22 ± 0.01
Apical, tubule	0.281 ± 0.006	5.0 ± 0.5				0.228 ± 0.006
Basolateral, tubule	0.242 ± 0.010	4.6 ± 0.3				0.218 ± 0.005

*Vesicle data were fit to a ground-state heterogeneity model; f_1 represents the fractional component arising from τ_1. Inclusion of ground-state heterogeneity did not improve the fit of the tubule data. Chi-squared values ranged from 0.69 to 4.0.

‡Multifrequency phase modulation data were fit to a single, hindered rotator model, with r_0 of 0.39 and lifetime of 6.7 ns. r_∞ for orientation-independent anisotropy decay data were calculated from the average of $r(t)$ from 10 to 20 ns after the flash, where $r(t)$ was constant. The rotational correlation time was under 1 ns.

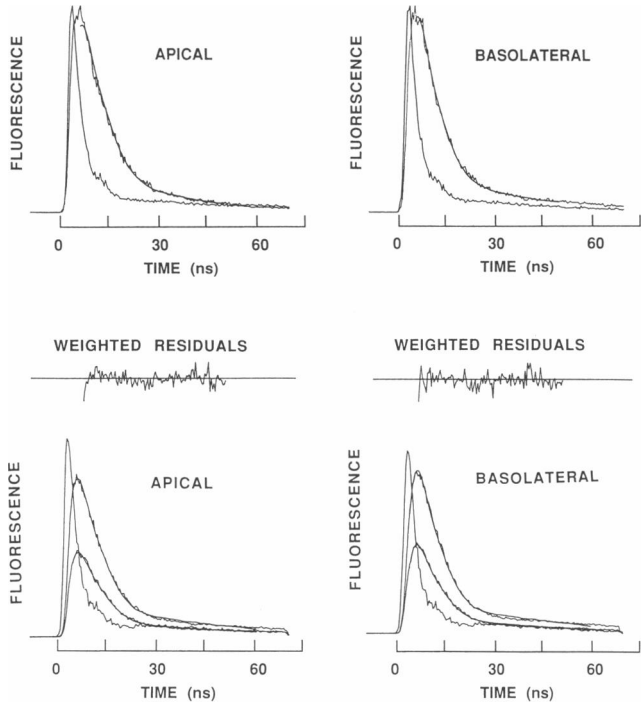

FIGURE 8 Fluorescence lifetime decay of proximal tubule labeled with TMA-DPH from the luminal and bath solutions. Fluorescence of a 100-μm segment of tubule was measured by a pulsed lifetime apparatus interfaced to the epifluorescence microscope as described in Methods. (*Top*) Lifetime decays in the absence of polarizers. The smooth curves through the data are a fit of a single exponential decay convoluted with the lamp profile (*narrow curves*). Fitted lifetimes and χ^2 values are: 4.39 ± 0.07 ns and 0.84 (basolateral membrane), and 4.98 ± 0.07 ns and 0.95 (apical membrane). (*Bottom*) Orientation-independent anisotropy decays were measured as described in the text. Parallel (*high broad curves*) and perpendicular (*low broad curves*) components of the fluorescence decay are given along with the flash lamp profile (*narrow curves*). Fitted r_∞ values are given in Table 3.

the image pixel intensities were replaced by intensities at nanosecond times. Fitted results are given in Fig. 8 (*bottom*), and listed in Table 3.[2] Limiting anisotropy values (r_∞) were similar to those measured in membrane vesicles. r_∞ for the apical membrane was slightly greater than that of the basolateral membrane, consistent with a higher fluidity in the basolateral membrane. The rotational correlation times were <1 ns and not well-determined in this study.

DISCUSSION

The purpose of these studies was to develop a quantitative imaging technique to map membrane fluidity in a complex polarized epithelium, the renal proximal tubule. Membrane fluidity was assessed from the steady-state fluorescence anisotropy of the membrane impermeable, fluidity-sensitive fluorophore TMA-DPH. TMA-DPH and related compounds have been used extensively to study membrane fluidity in biological membranes, however, previous measurements of fluorophore anisotropy have been made by spatial averaging in macroscopic samples. In this study the apical and basolateral membranes of the isolated perfused kidney proximal tubule were labeled individually by addition of TMA-DPH to the luminal or bath solutions. TMA-DPH did not undergo significant internalization, nor did it move across the tight junction joining the apical membranes of adjacent cells to label the contralateral plasma membrane. The fluorescence anisotropy of TMA-DPH was stable in time and independent of the concentration of TMA-DPH in the perfusion solutions over the range of concentrations used.

To measure fluorescence anisotropy with spatial resolution, rotatable excitation and emission polarizers were incorporated into an inverted epifluorescence microscope with detection by an image intensifier and CCD camera. The choice of microscope components was particularly important to minimize polarization artifacts and background autofluorescence. All glass optics were replaced by fused silica, and lenses with long focal length required for parfocality and for protection of the filter cube were removed. The selection of a dichroic mirror was a major concern. The reflection and transmission characteristics for polarized light are a complex function of wavelength, polarization direction, dichroic angle, and the dichroic composition and coating. For use with TMA-DPH, a 400-nm fused silica dichroic mirror was found empirically to have the least polarization artifacts. Nevertheless, it was necessary to make corrections for the differential transmission and depolarization artifacts of the dichroic mirror. The correction procedure was validated from the independence of anisotropy of randomly oriented fluorophores on the angle of excitation polarized light. Most of the experiments were performed with a 40× quartz objective with NA 0.65; comparison of data obtained by use of NA 0.35 and 1.30 objectives showed little artifacts from objective depolarization by use of the quartz objective.

[2]The accuracy limits of time-resolved, orientation-independent anisotropy were evaluated as in Appendix 2. The final expression from Eq. A-9 was integrated over γ to emulate the experimental situation where spatially averaged fluorescence was measured. Calculated anisotropy was $r = [4(3 + 2a^2 + 2b^2)(3\cos^2\alpha - 1)]/[3(2 - a^2 - b^2)\cos^2\alpha + 54 + 43a^2 + 43b^2]$, where a and b are defined in Appendix 2. When $\alpha = 0$, r is 0.4 as predicted. When α is 30°, this equation shows that the maximal error in the estimation of r_{ran}, $(3\cos^2\alpha - 1)/5$, is 2.5%. Even if α were 60°, the maximal error becomes 7.5%. Therefore, there is little error in the determination of the limiting anisotropy (r_∞) when anisotropy decay measurements are performed by the orientation-independent method.

The red end of the TMA-DPH excitation spectrum (380 nm) was chosen to minimize autofluorescence and photodynamic tubule injury. Tubules were illuminated at low intensity using a tungsten-halogen lamp having little output at wavelengths below 400 nm. In addition, tubules were illuminated only during the measurement process. Under these conditions, no photobleaching or photodynamic tubule injury were observed.

The anisotropy images of the labeled tubule, obtained using a single plane of excitation polarization, showed a dramatic dependence of measured anisotropy on tubule orientation. It was necessary to eliminate this dependence to derive physical meaning from measured anisotropy values. Tubules were illuminated with different planes of excitation polarization between 0° and 180°. It was shown mathematically that the dependence of measured anisotropy on fluorophore orientation in the x-z plane was eliminated effectively by integration of the parallel and perpendicular components of emitted fluorescence over a 180° angle of excitation polarization. This method worked in practice, as demonstrated by the independence of anisotropy along the length of tubule in Fig. 6.

The theory showed that in general the orientation-independent anisotropy image is not the true anisotropy (r_{ran}) that would be measured if the fluorophore were oriented randomly in three dimensions. This is easily understood for a fluorophore oriented parallel to phospholipids in a spherical cell. The component of the excitation dipole along the y-axis is a function of position along the surface of the sphere; the measured anisotropy would be given by Eq. 4 as plotted in Fig. 5. In the special case of the cylindrical kidney tubule, it was possible to establish strict limits on the error in the determination of r_{ran}, and to correct measured r for out-of-plane fluorophore orientations. Based on the analysis in Appendix 2, and the similar lifetimes of TMA-DPH in the apical and basolateral membranes of the intact proximal tubule, it is concluded that apical membrane fluidity is significantly lower than basolateral membrane fluidity.

There have been several studies of membrane fluidity in isolated apical and basolateral vesicles from kidney proximal tubule. Studies of the steady-state fluorescence anisotropy of DPH and its analogues generally show that the fluidity of the apical membrane is slightly higher than that of the basolateral membrane (Le Grimellec et al., 1983; Hise et al., 1984; Verkman and Ives, 1986). Time-resolved measurements of parinaric acids showed that the gel–fluid phase structure of the opposing apical and basolateral membranes differ significantly (Illsley et al., 1988). Our results obtained in the viable perfused proximal tubule show much larger differences between apical and basolateral fluidity, as assessed by steady-state TMA-DPH anisotropy measurements, than do vesicle studies. The reasons for this difference may be contamination of the vesicle preparation with other cellular membranes or modification of the vesicle membrane during the isolation procedure. Results in the intact tubule are insensitive to these significant difficulties. In addition, the unique intracellular milieu adjacent to the plasma membrane and active membrane biochemistry are not preserved in vesicle studies.

Fluorescence lifetime studies were performed to investigate whether differences in TMA-DPH steady-state anisotropy between apical and basolateral membranes were due to changes in lifetime or in rotational mobility. Phase-modulation measurements in isolated membrane vesicles showed similar TMA-DPH lifetimes in apical and basolateral membrane vesicles; rotation of TMA-DPH in both types of vesicles was described reasonably well by a single hindered rotator anisotropy decay model with a restricted angle of rotation of ~31°. Lifetime microscopy studies in the intact tubule were performed using a pulsed excitation source and gated-photomultiplier detection. Lifetimes of TMA-DPH in the apical and basolateral membranes of the intact perfused tubule did not differ significantly, providing support for the interpretation of anisotropy differences in terms of fluidity differences. In membranes, the steady-state anisotropy of DPH and its analogues has been found to parallel the limiting anisotropy values. Both the steady-state and time-resolved analyses indicate higher basolateral than apical membrane fluidity.

In summary, we have examined the membrane fluidity of the apical and basolateral cell plasma membranes of the intact proximal tubule by a new imaging method. Unlike studies in isolated membrane vesicles, fluidity measurements in the intact tubule are not influenced by impurity or preparation artifacts, and can be used to measure differences and changes in fluidity in real-time. This approach should have important applications to examine the role of fluidity in the transduction of a variety of regulatory signals in intact epithelial cells.

APPENDIX 1: CALCULATION OF ANISOTROPY PROFILE FOR APICAL MEMBRANE LABELING

The measured anisotropy across the tubule image is calculated theoretically for luminal loading of TMA-DPH. We first obtain an expression for $I_\parallel$ and $I_\perp$ for excitation light polarized in the y-z and x-y planes by integrating the integrands in Eq. 2 over the angles θ, ϕ, and β with $D(\theta, \phi)$ defining a radial fluorophore distribution as depicted in Fig. 3.

y-z polarization ($\psi = 0°$):

$$I_\parallel = (\pi^2/4)(5\cos^2\alpha + 1)$$
$$I_\perp = (\pi^2/4)[-(3\cos^2\gamma + 1)\cos^2\alpha + \cos^2\gamma + 3] \quad \text{(A-1)}$$

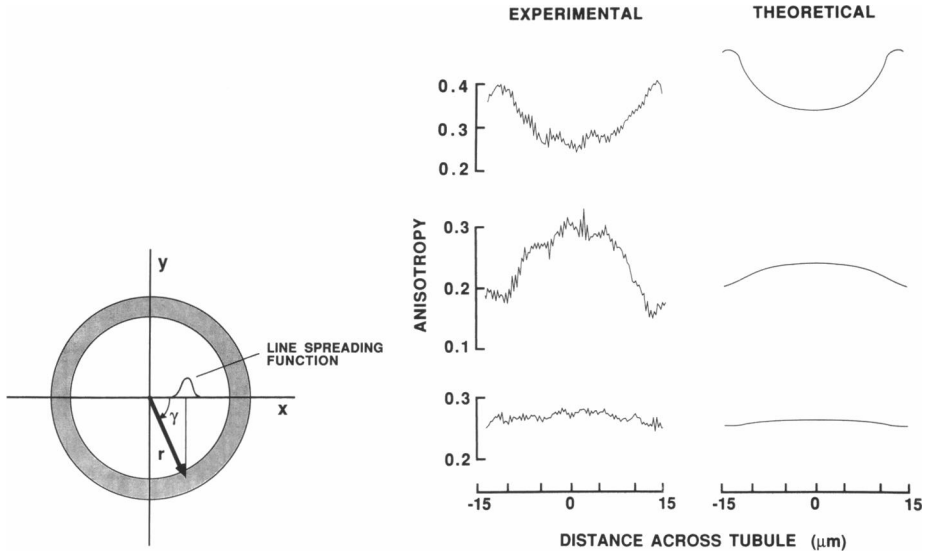

FIGURE 9 Experimental and theoretical anisotropy profiles of TMA-DPH across the tubule labeled from the lumen. (Left) Cross-section of tubule. TMA-DPH is assumed to be located in an annulus from 12 to 15 μm from the center of the tubule. Excitation light propagates in the y-direction; x-z is the focal plane. Light is polarized in the z-y and x-y planes. The fluorescence intensity for point (r, γ) is given by Eqs. A-1, A-2, and A-3. The line-spreading function projects this point onto the x-axis; the width of the spreading function increases as the distance from the focal plane increases. (Right) Experimental and theoretical anisotropy profiles across the tubule. Excitation polarization is in the z-y plane (*top curves*) and x-y plane (*middle curves*). The orientation-independent anisotropy profile is given in the bottom curves. See Appendix for details.

x-y polarization ($\psi = 90°$):

$$I_\parallel = (\pi^2/4)[(\cos^2\gamma - 1)(13\cos^2\gamma - 5)\cos^2\alpha - (7\cos^2\gamma + 1)(\cos^2\gamma - 1)]$$
$$I_\perp = (\pi^2/4)[(\cos^2\gamma - 1)\cos^2\alpha - 3(\cos^2\gamma - 1)] \quad \text{(A-2)}$$

Orientation-independent values for $I_\parallel$ and $I_\perp$ are calculated by integration of the expression for $I_\parallel(\psi)$ and $I_\perp(\psi)$ over ψ:

$$I_\parallel = (\pi^3/16)[(27\cos^4\gamma - 56\cos^2\gamma + 40)\cos^2\alpha - 9\cos^4\gamma + 8\cos^2\gamma + 8]$$
$$I_\perp = (\pi^3/16)[(9\cos^4\gamma - 8\cos^2\gamma - 8)\cos^2\alpha - 3\cos^4\gamma - 8\cos^2\gamma + 24]. \quad \text{(A-3)}$$

These equations express $I_\parallel$ and $I_\perp$ as a function of the angle γ as defined in Figs. 3 and 9. The brush border is taken to be an annulus from r = 12–15 μm; the TMA-DPH fluorescence is assumed to be radially uniform in the annulus.

To calculate the spatial distribution of emitted fluorescence along the x-axis in the focal plane [$I(x)$], a line-spreading function, $L(x', y')$, was used to propagate intensities from out-of-focus points:

$$I_k(x) = I_k(r, \gamma)L(x', y'), \quad \text{(A-4)}$$

where k denotes the parallel or perpendicular component of fluorescence. The line-spreading function was measured by imaging an aqueous solution of 100 μM SPA in a 0.5-μm glass capillary tube. $L(x, y)$ was parameterized for points above the focal plane by a single Gaussian function whose width depended on the distance y' above the focal plane,

$$L(x', y') = \exp[(x' - x)^2/(0.53y')^2] \quad \text{(A-5)}$$

or, for points below the focal plane, by the sum of three Gaussian functions whose offset and width depended on the distance below the focal plane

$$L(x', y') = \sum_{i=-1}^{1} \exp[(x' - 0.45y'i - x)^2/(0.53y')^2]. \quad \text{(A-6)}$$

In these equations, the fluorescence from a point (x', y') inside the annulus is projected onto the x-axis (see Fig. 9). The factors 0.53 and 0.45 were determined from the distribution of fluorescence intensity across the image of the capillary tube for seven different heights above and below the focal plane using the 100× objective.

The simulation was performed by integrating numerically over γ and r_1 = 12–15 μm:

$$I_k(x) = \frac{\int_0^\pi d\gamma \int_{r_1}^{r_2} dr\, I_k(r, \gamma)L(x', y')}{\int_0^\pi d\gamma \int_{r_1}^{r_2} dr\, L(x', y')}. \quad \text{(A-7)}$$

The anisotropy across the tubule, $r(x)$, was calculated from the expression, $r(x) = [I_\parallel(x) - I_\perp(x)]/[I_\parallel(x) + 2I_\perp(x)]$.

Fig. 9 shows experimental values of $r(x)$ obtained by integrating anisotropy images across the tubule obtained with excitation light polarized in the y-z and x-y planes, and from orientation-independent integration. A value of $\cos^2\alpha$ = 0.76 (29°) was estimated by minimizing the difference between experimental and calculated $r(x)$.

APPENDIX 2: TUBULE r CALCULATED FOR GENERALIZED ORIENTATION DISTRIBUTION

Tubule r is calculated for a generalized orientation distribution function, $D(\theta, \phi)$, described by parameters a and b. $D(\theta, \phi)$ was chosen so that resultant integrals were solvable analytically. Defining $D(\theta, \phi) = (x^2 + y^2 + z^2)^{-1}$, where $a^2x^2 + b^2y^2 + z^2 = 1$, and taking the tubule axis along the z-axis (see Figs. 3 and 4),

$$D(\theta, \phi, \gamma) = a^2 \sin^2\theta \sin^2(\phi - \gamma) + b^2 \sin^2\theta \cos^2(\phi - \gamma) + \cos^2\theta. \quad \text{(A-8)}$$

The parallel polarization component is calculated for the orientation-independent anisotropy image as,

$$I_{\parallel} = \int_0^{\pi} d\theta \int_0^{2\pi} d\phi \int_0^{2\pi} d\beta \int_0^{\pi} d\psi \, (\mathbf{F}_{ex} \cdot \mathbf{x}')^2 (\mathbf{F}_{em} \cdot \mathbf{z}')^2 D(\theta, \phi, \gamma) \sin\theta, \quad \text{(A-9)}$$

where $\mathbf{F}_{ex}$, $\mathbf{F}_{em}$ and $\mathbf{z}'$ are defined in Eq. 1. $I_{\perp}$ is calculated by replacement of $(\mathbf{F}_{ex} \cdot \mathbf{z}')^2$ by $(\mathbf{F}_{em} \cdot \mathbf{x}')^2$.

The four integrals in Eq. A-9 contain 270 terms, each of which contain sine and cosine functions, up to the sixth power, of θ, ϕ, γ, ψ, α, and β. When expressed as cosine functions of individual angles, this becomes 3,640 terms with a total of ~11,000 cosine functions. General computer software was constructed to evaluate this type of integral analytically (BASIC program available on request). At the "edge" ($\gamma = 0$) and "center" ($\gamma = \pi/2$) of the tubule,

$$r(\gamma = 0) = \frac{(18 + 6a^2 + 18b^2)\cos^2\alpha - 6 - 2a^2 - 6b^2}{(3 - 6a^2 + 3b^2)\cos^2\alpha + 27 + 16a^2 + 27b^2}$$

$$r(\gamma = \pi/2) = \frac{(18 + 18a^2 + 6b^2)\cos^2\alpha - 6 - 6a^2 - 2b^2}{(3 + 3a^2 - 6b^2)\cos^2\alpha + 27 + 27a^2 + 16b^2}. \quad \text{(A-10)}$$

The theoretical maximum and minimum limits on r were determined from Eq. A-10 to be 0.276–0.315 using $\cos^2\alpha = 0.802$ (apical membrane) and 0.237 – 0.282 using $\cos^2\alpha = 0.740$ (basolateral membrane). This calculation shows that r_{ran} must be within these limits when α is calculated from measured r.

To correct measured r formally for out-of-plane effects, a and b were determined by a nonlinear fitting procedure, making use of the measured r at the edge and center of the tubule for the anisotropy images measured at two different planes of excitation polarization ($\psi = 0$ and $\pi/2$). Expressions for r as in Eq. A-10 were derived with inclusion of a delta function (setting $\gamma = 0$, or $\pi/2$) in Eq. A-9. For the apical membrane, $a^2 = 0.166$ and $b^2 = 1.22$; measured $r = 0.278$–0.283 (center-edge of tubule) was corrected to 0.281. For the basolateral membrane, $a^2 = 1.480$ and $b^2 = 0.552$; measured $r = 0.240 - 0.247$ was corrected to 0.244. These calculations show that corrected r (which should be r_{ran}) falls within the narrow range of r measured across the tubule in the orientation-independent anisotropy image.

This work was supported by grants DK35124, DK39354, and HL42368 from the National Institutes of Health, a grant-in-aid from the American Heart Association, and a grant from the National Cystic Fibrosis Foundation. Dr. Verkman is an Established Investigator of the American Heart Association. Dr. Fushimi is a Fellow of the National Kidney Foundation.

Received for publication 25 May 1989 and in final form 22 September 1989

REFERENCES

Axelrod, D. 1979. Carbocyanine dye orientation in red cell membrane studied by microscopic fluorescence polarization. *Biophys. J.* 26:557–574.

Axelrod, D. 1989. Fluorescence polarization microscopy. *Methods Cell Biol.* 30:333–352.

Berry, C. A., and A. S. Verkman. 1988. Osmotic gradient dependence of osmotic water permeability in the rabbit proximal convoluted tubule. *J. Membr. Biol.* 105:33–43.

Brasitus, T. A., P. K. Dudeja, H. J. Worman, and E. S. Foster. 1986. The lipid fluidity of rat colonic brush-border membrane vesicles modulates Na^+-H^+ exchange and osmotic water permeability. *Biochim. Biophys. Acta.* 855:16–24.

Brasitus, T. A., K.-Y. Yeh, P. R. Holt, and D. Schachter. 1984. Lipid fluidity and composition of intestinal microvillus membranes isolated from rats of different ages. *Biochim. Biophys. Acta.* 778:341–348.

Burghardt, T. P. 1984. Model-independent fluorescence polarization for measuring order in a biological assembly. *Biopolymers.* 23:2383–2406.

Calafut, T. M., J. A. Dix, and A. S. Verkman. 1989. Fluorescence depolarization of *cis*- and *trans*-parinaric acids in artificial and red cell membranes resolved by a double hindered rotational model. *Biochemistry.* 28:5051–5058.

Chesney, R. W., N. Gusowski, and I. Zelikovic. 1986. Membrane fluidity and phospholipid composition in relation to sulfur amino acid intake in brush border membranes of rat kidney. *Prediatr. Res.* 20:1305–1309.

Dix, J. A., and A. S. Verkman. 1990. Spatially-resolved mapping of fluorescence anisotropy in single cells: application to cytoplasmic viscosity. *Biophys. J.* 57:231–240.

Engel, L. W., and F. G. Prendergast. 1981. Values for and significance of order parameters and "cone angles" of fluorophore rotation in lipid bilayers. *Biochemistry.* 20:7338–7345.

Hise, M. K., W. W. Mantulin, and E. J. Weinman. 1984. Fluidity and composition of brush border and basolateral membranes from rat kidney. *Am. J. Physiol.* 247:F434–F439.

Illsley, N. P., H. Y. Lin, and A. S. Verkman. 1988. Lipid-phase structure in epithelial cell membranes: comparison of renal brush border and basolateral membranes. *Biochemistry.* 27:2077–2083.

Kaissling, B., and W. Kriz. 1979. Structural analysis of the rabbit kidney. *Adv. Anat. Embryol. Cell Biol.* 56:1–32.

Kuwahara, M., C. A. Berry, and A. S. Verkman. 1988. Rapid development of vasopressin-induced hydroosmosis in kidney collecting tubules measured by a new fluorescence technique. *Biophys. J.* 54:595–602.

LeGrimellec, C., S. Carriere, J. Cardinal, and M.-C. Giocondi. 1983. Fluidity of brush border and basolateral membranes from human kidney cortex. *Am. J. Physiol.* 245:F227–F231.

LeGrimellec, G., G. Friedlander, and M.-C. Giocondi. 1988. Asymmetry of plasma membrane lipid order in Madin-Darby canine kidney cells. *Am. J. Physiol.* 255:F22–F32.

Medow, M. S., and S. Segal. 1987. Age related changes in fluidity of rat renal brushborder membrane vesicles. *Biochem. Biophys. Res. Commun.* 142:849–856.

Molitoris, B. A., and C. Hoilien. 1987. Static and dynamic components of renal cortical brush border and basolateral membrane fluidity: role of cholesterol. *J. Membr. Biol.* 99:165–172.

Prendergast, F. G., R. P. Haugland, and P. J. Callahan. 1981. 1-[4-(Trimethylamino)phenyl]-6-phenylhexa-1,3,5-triene: synthesis, fluorescence properties, and use as a fluorescence probe of lipid bilayers. *Biochemistry.* 20:7333–7338.

Strange, K., and K. R. Spring. 1986. Methods for imaging renal tubule cells. *Kidney Int.* 30:192–200.

van Gurp, M., G. van Gindel, and Y. K. Levine. 1988. Orientational properties of biological pigments in ordered systems studied with polarized light: photosynthetic pigment-protein complexes in membranes. *J. Theor. Biol.* 131:333–349.

Verkman, A. S., and H. E. Ives. 1986. Water permeability and fluidity of renal basolateral membranes. *Am. J. Physiol.* 250:F633–F643.